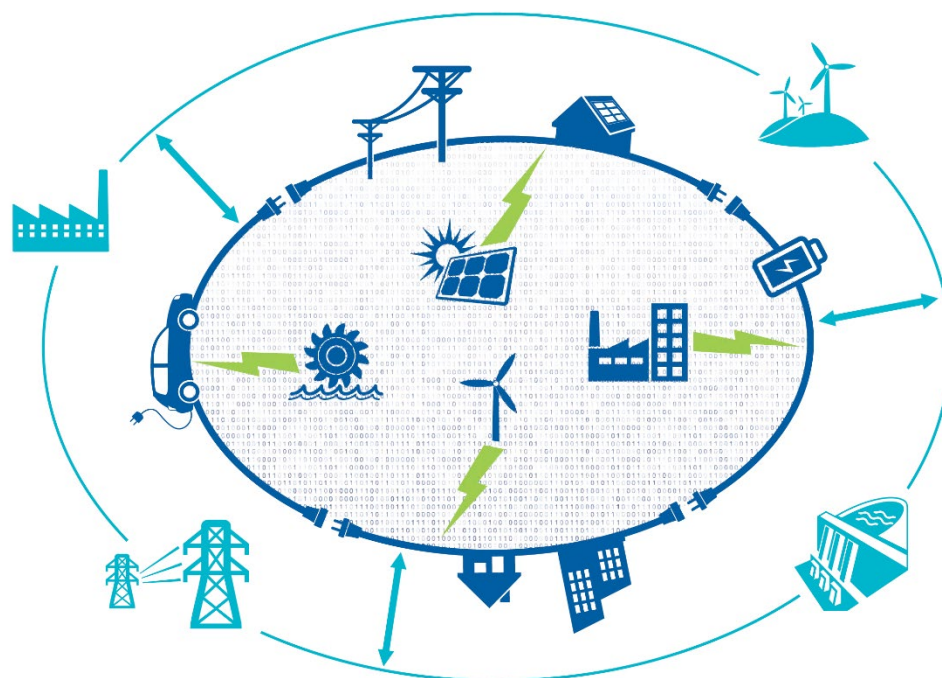# Case study: Challenges and possible measures in the future Norwegian distribution grid

Authors: Ivar Bjerkebæk, Stine Ekrheim

CINELDI

Centre for intelligent electricity distribution
- to empower the future Smart Grid

Centres for
Environment-friendly
Energy Research

CINELDI - Centre for intelligent electricity distribution

The research centre is financed by the Research Council of Norway and the Norwegian partners through the Centre for Environment-friendly Energy Research (FME) scheme. The FME scheme consists of research centres of limited duration that conduct concentrated, focused and long-term research on a high international level to solve specific challenges related to energy and the environment.

TITLE	
Case study: Challenges and possible measures in the future Norwegian distribution grid	
AUTHOR(S)	
Ivar Bjerkebæk and Stine Ekrheim, SINTEF Energi AS	

EXECUTIVE SUMMARY
This case study aims to illustrate challenges and possible measures in a future Norwegian distribution grid in 2030-40. Based on official goals by the Norwegian government and the EU to decarbonize transport and increase the amount of distributed renewable energy production, we consider a future scenario where the distribution grid is subject to considerable increase in photovoltaic (PV) production and electric vehicle (EV) charging. If no action is taken, the expected changes in load and production will lead to violation of voltage limits and thermal overload on components. Through simulations, we show how these problems can be mitigated by using a combination of active measures in the grid and flexibility resources. The case study is built on tools and knowledge from CINELDI and affiliated research projects.

QUALITY ASSURANCE		
Main author	Ivar Bjerkebæk	*Ivar Bjerkebæk (Dec 2, 2024 10:46 GMT+1)*
WP leader	Gerd Kjølle	*Gerd Kjølle*
Centre director	Gerd Kjølle	
Scientific coordinator	Vijay Venu Vadlamudi	

VERSION NO	DATE	VERSION DESCRIPTION
1.0	2024-11-28	Final version

Table of Contents

1   Introduction

The case study presented in this report aims to illustrate a future Norwegian distribution grid in 2030-40. Based on official goals by the Norwegian government and the EU to decarbonize transport and increase the amount of distributed renewable energy production, we consider a future scenario where the distribution grid is subject to considerable increase in photovoltaic (PV) production and electric vehicle (EV) charging. If no action is taken, the expected changes in load and production will lead to violation of voltage limits and thermal overload on components. We investigate whether these problems can be mitigated, without grid reinforcement, by using a combination of active measures in the grid and flexibility resources.

The case study makes use of tools and knowledge acquired in CINELDI and affiliated research projects and is based on numerical simulations on a test system. The test system is an interconnected 22kV medium voltage (MV) grid and a 400V low voltage (LV) grid. The MV grid is represented by the CINELDI MV reference grid [1], and the LV grid is represented by the residential radial of the CIGRE Benchmark LV grid [2]. The future scenario with new loads and production is constructed based on the following targets announced by the Norwegian Government and the EU:

1. In 2025 all sold private cars in Norway must be electric [3].
2. All new heavy duty vehicles sold in 2030 in Norway have zero-emissions [4].
3. The annual PV production in Norway in 2030 is 8 TWh [5].
4. According to the European Solar Rooftops Initiative, all new buildings should be "solar ready" in 2030 [6].
5. The EUs Energy Efficiency Directive (EED) sets a target of 11.7% reduction in energy consumption by 2030 compared to 2020 levels [7].

Considering point 1-2 we include fast charging stations (FCS) for EVs and high-power charging stations (HPCS) for heavy duty vehicles in the future grid. Considering point 3-4 we add PV panels on all rooftops in the LV grid, and we include a larger PV-plant in the MV grid. The final point on energy consumption highlights the importance of electric losses, therefore we study how each new element introduced in the case affects the losses.

The case study is presented in three parts. In the first part, rooftop PV in a single LV radial is studied. In part 2, the effect of rooftop PV is studied in the interconnected MV grid with multiple LV radials. Whereas part 1-2 considered new production at the LV level, part 3 adds new loads and production on the MV level. A summary of the three parts of the case is given in Table 1. For all three parts, the electrical loss in the system will be considered.

Table 1: Summary of the three parts of the case study describing the load and production elements, the types of grid problems encountered, and which solutions were considered to mitigate these problems.

Grid Level	Load/production	Grid problem	Chosen solution(s)
LV	Rooftop PV on residential buildings	Voltage problems (high voltage)	3 alternatives considered: 1) Manual tap changer (NLTC) 2) Automatic tap changer (OLTC) 3) Automatic curtailment.
MV/LV	Rooftop PV on all residential buildings in the interconnected MV/LV grid.	Voltage problems (high voltage)	Automatic tap changer (OLTC) on LV side of transformers.
MV/LV	PV plant, FCSs and a HPCS connected to the MV grid. The rooftop PV from part 1-2 is included.	Voltage problems (low voltage and high voltage) Thermal overload on power lines.	Automatic tap changer (OLTC) on LV side of transformers. Battery energy storage system (BESS).

The remainder of the document is structured as follows: Chapter 2 describes the test system. Chapter 3-5 covers the results from the three parts of the case study corresponding to Table 1. Chapter 3-5 describes the main assumptions used in the case study, but a more detailed description of the chosen simulation methods is left for Appendix A. In chapter 6, the electrical loss for all the parts in the case study is assessed.

2   Description of the test system

The test system consists of a medium voltage (22kV) grid with LV (400V) radials connected at two different locations. The remaining load points in the MV grid represent the aggregated load from customers in LV circuits, or industrial loads. These LV grids are not explicitly modelled. The open source tool *pandapower* [8] is used for power flow calculations on the test system.

2.1   Medium voltage grid

The CINELDI MV reference grid is used to model the medium voltage grid in this case study. The grid is a 22kV radial grid with 124 buses and is representative for a Norwegian medium voltage distribution grid. A total of 54 buses are pre-existing load points. The load points represent secondary substations transforming the voltage to $230V$ or $400V$, and the provided load profiles associated to each load point are one year of aggregated AMS data for all customers connected to the same transformer. The dataset for the reference grid is described in detail in reference [9].
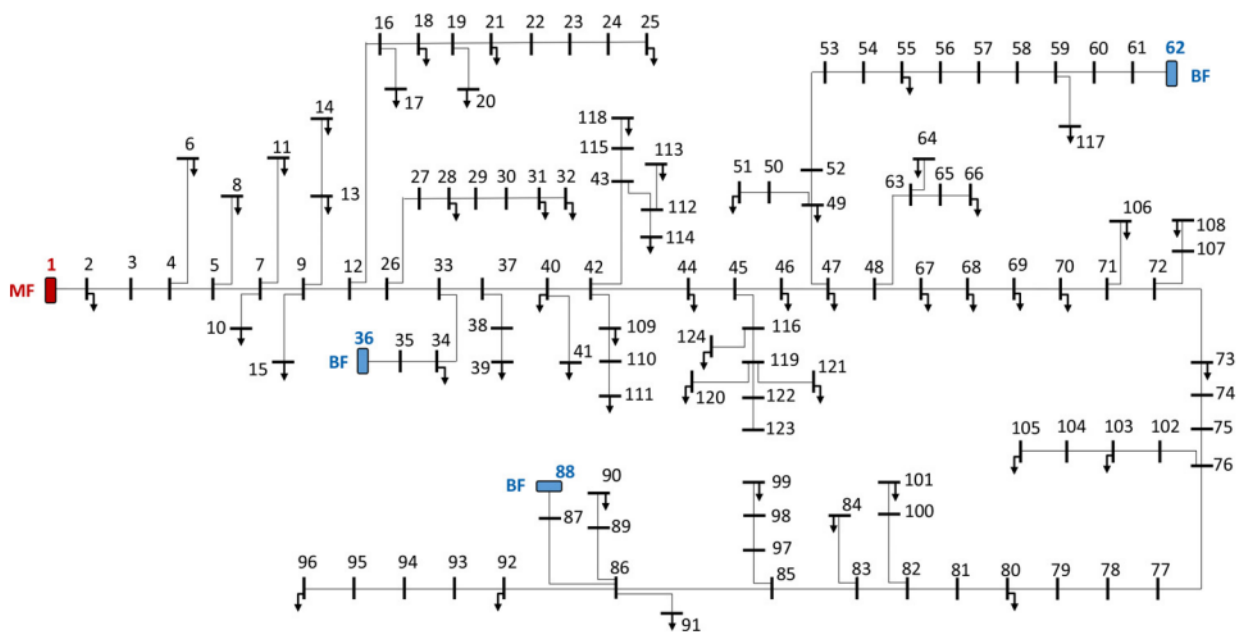

Figure 1: CINELDI MV reference grid [9]. The main feeder (MF) marks the main transformer connecting to the regional transmission grid. Alternative connections are marked as backup feeders (BF) and are not used in this case study. Preexisting load points are marked with vertical arrows.

2.2   Low voltage grid

The low voltage grid that is used is a modified version of the CIGRE Benchmark European LV grid [10], the topology of the grid is shown in Figure 2 and it consists of a residential subnetwork, an industrial subnetwork and a commercial subnetwork. The modification that has been done, is that only the residential part of the grid is considered, the line lengths are increased, and the nominal voltage at the high voltage side of the transformer is set to 22 kV to match the MV grid. In this case study we will connect the LV grid to two of the buses with load in the MV grid. To be able to do that, the aggregate

load in the LV grid should match the load on the connecting bus. One possibility is to scale the loads in the LV grid. However, this will impact the properties of the grid in terms of voltage drops and possible overloads and may cause the grid to be either over- or under-dimensioned. To demonstrate the interaction between the MV and the LV grid, we have chosen to add the detailed LV grid only bus to 49 and bus 101. To match the MV grid loads, the load on bus bar R1 is removed for the LV grid connected to bus 101 as this is connected right after the transformer and will not influence the voltage drop over the individual lines in the LV grid. In the dataset for the LV grid, only the maximum value of the load on all the buses are provided. To get one year of data (like the MV grid), we assume that the coincidence factor is 1, which implies that all loads have the maximum load at the same time, and the timeseries are projected from the MV grid to the LV grid.
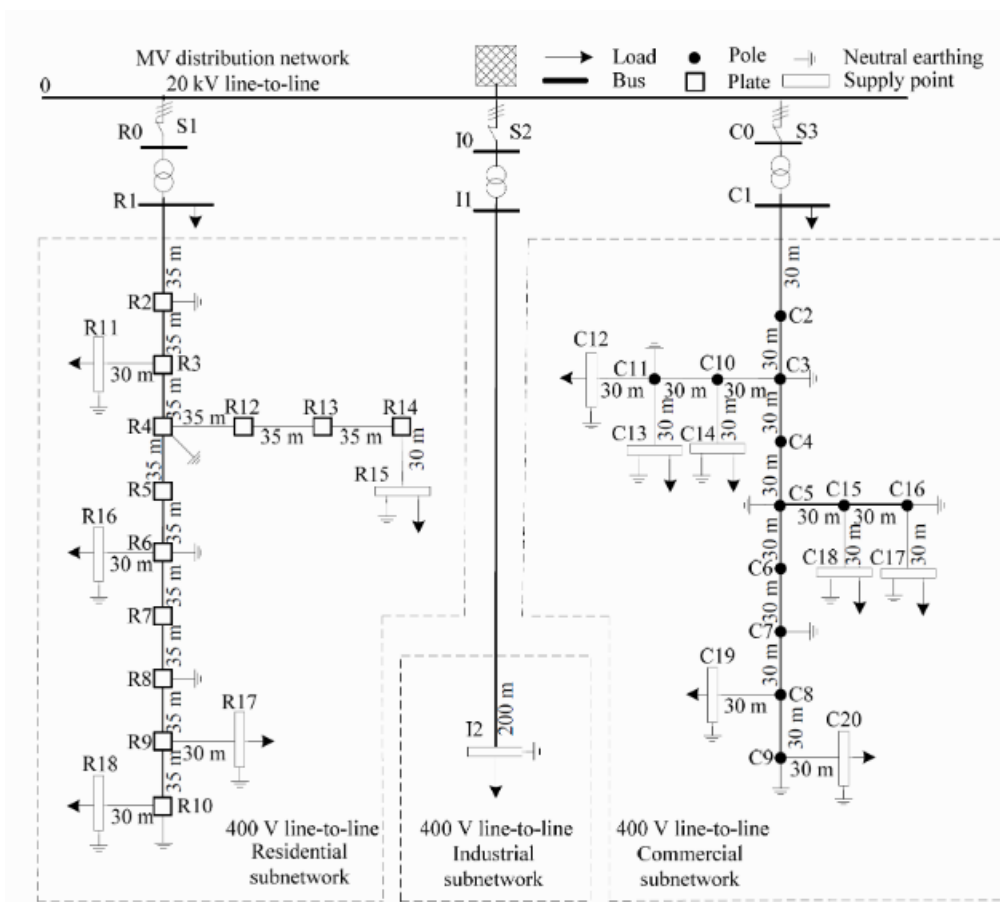

Figure 2: Topology of European LV distribution network benchmark [10].

To avoid violation of the lower voltage limit in the hours with a high load demand, the tap setting of the transformers must be suitably adjusted. Today there is normally either one tap level all year round, or one tap level for winter season and one for the summer season. In this case study, two tap levels a year is assumed. Normally the changing of tap level is done with a no-load-tap-changer (NLTC), this may be challenging as it means that the load needs to be disconnected to change the tap-position. For grid companies spanning over a big area, seasonal tap-changing may be very time consuming, and therefore this assumption may overestimate the typical ability to cope with seasonal load variations. Nevertheless, in this case study a NLTC is assumed. The tap levels in the different seasons (winter and summer), are decided based on the hour with the highest load demand in that period. The tap-changer steps are 2.5 %, and for the case study suitable tap-changer levels are found to be 7.5 % in the winter, and 0 % in the summer, for both the LV grids at bus 49 and 101.

2.3 PV production

To model the new loads in the system both external tools and results obtained in CINELDI, and affiliated research projects are used. PV panels on rooftops are studied earlier in the FINE project[1]. The aim of the FINE project is to research how local energy communities can be flexibly integrated into the Norwegian power grid [11]. In this case study, many of the assumptions from the FINE study will be applied. One of these assumptions is that the average yearly energy demand per household is 15 MWh, this is based on data from Elhub [12]. This is used to estimate the number of households per load point in the LV grid. To model PV production a tool called *Renewables ninja* [13], [14] is used. This tool estimates hourly power produced given capacity on the PV panel, angle of the PV panel both related to the ground and cardinal direction, time and location. On average the installed capacity in a normal household is $9\ kW_p$ [15]. When adding solar panels to rooftops in this case study, the capacity is drawn from a normal distribution with an expectation value of $9\ kW_p$ and standard deviation of is $3\ kW_p$. The angles of the solar panels are kept constant at a 35° tilt and directed toward south.

To obtain some initial insights on the potential impact of PV production in the grid, we studied the temporal variation of the capacity factor, similar to what was done in reference [14]. For a PV panel situated in the Oslo-region, we acquired 30 years of production data from the Renewables Ninja platform and studied the daily variation of the capacity factor in summer and winter separately. The daily variation is visualized in Figure 3. The figure shows that one can expect to always have some production during a summer day. Midday in summer, the median capacity factor is 62%, and in 99% of the cases the capacity factor stays above 9% and below 83%. In winter, the median capacity factor is only 10% and zero-production midday is not unusual. Thus, one can expect the impact of PV production in winter to be almost negligible compared to the summer period.
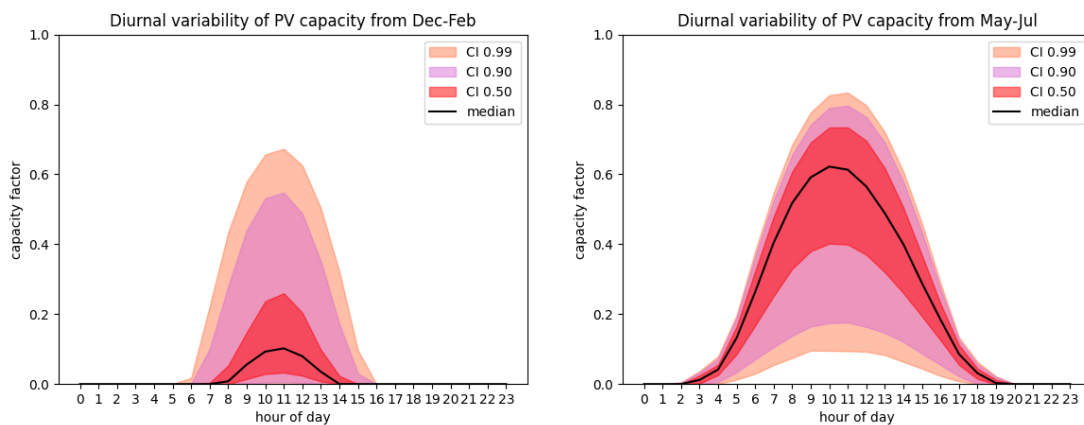

Figure 3: Diurnal variability of PV production in December to February (left) and May to July (right). The median capacity per hour of the day is plotted as a black line, and quantile ranges are shown in shades of red.

---

[1] FINE: Flexible Integration of Local Energy Communities into the Norwegian Electricity Distribution System, https://www.sintef.no/en/projects/2020/fine/

2.4 Load data for charging stations

The load demand for charging stations is obtained from FuChar [2]. The FuChar project goal is to minimise investment and operating costs related to the grid integration of electric transport. The load data for the fast-charging station (FCS) is modelled based on measured data. From this we can get an hourly load timeseries for the load demand from the FCS. For the charging stations for heavy-duty vehicles, there is not yet much charging pattern data available. Because of this, the load demand for a charging station for these vehicles are modelled based on traffic flow and battery size [16]. The load profile for one day for charging of both private cars and the heavy-duty transportation, that is used in this case, is shown in Figure 4. For the HPCS, this profile is the same for every day in the modelled year, but for the FCS this profile is dependent on weekday and month.
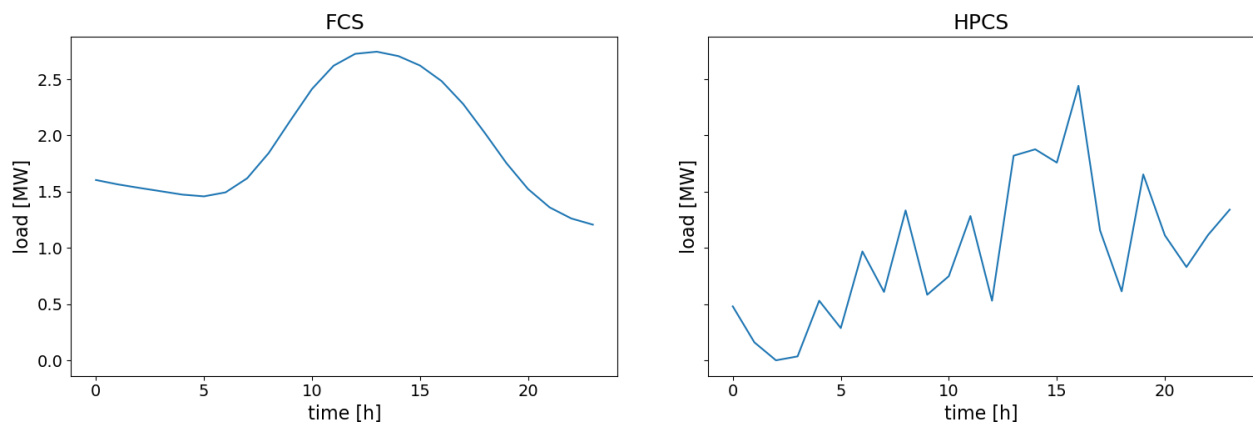

Figure 4: Daily load curve for modelled data for FCS (left) and HPCS (right).

---

[2] FuChar: Grid and Charging Infrastructure of the Future, https://www.sintef.no/prosjekter/2019/fuchar/

3 PV in the LV grid

The first scenario in the case study is to look at PV on residential rooftops in the LV grid. If no active measures are taken, simulations show that adding PV panels on all rooftops will lead to violation of the upper voltage limit. The thermal capacity on the transformer could also be a problem in this case, but it is assumed that the transformers have sufficient capacity in the future grid. There are several ways to avoid violation of the voltage limits, and in this case study three approaches will be considered.

The first option is to limit the amount of PV by adding PV panels on rooftops only until the voltage gets too high. This is done by adding PV on rooftops one by one randomly. Since the capacity of the PV installations are drawn from a normal distribution and since the position in the grid matters, this is done multiple times to obtain an average value of the hosting capacity and the corresponding yearly energy production.

The second option considered is adding PVs on all rooftops and curtailing the production when the voltage gets too high. This is modelled by looking at how high the power flow to the upstream grid can be before the voltage levels become too high. The PV production is curtailed when the export from the LV grid exceeds the limit. How the curtailment is done is explained in more detail in Appendix A.1.

Lastly, automatic on-load-tap-changers (OLTC) was considered. OLTC makes the tap-changing more accessible, since the load does not have to be disconnected during operation compared to the no-load-tap-changer. The on-load-tap-changing can also be done automatically compared to the NLTC that is operated manually. For this case it is assumed that the tap-changing steps are 1%, and that the maximum and minimum tap settings are $\pm10\%$. The method that was used for determining the tap setting at each time step is described in Appendix A.2.

3.1 Results

The total installed capacity, total annual produced energy and total annual loss for the different cases and the two different LV grids is given in Table 2. The results show that for the first case between 20 to 30 % of the households can install PV before there are problems, for both the LV grids. This number is slightly higher for the LV grid at bus 49. For the two cases with curtailment and OLTC, PV cells can be installed on all rooftops, and the resulting installed capacity is therefore the same.

The differences between the cases with curtailment and OLTC are in the produced energy and the total losses. When curtailing the solar production instead of using an OLTC, the production is 20 % and 15% less, for LV grids at bus 49 and bus 101 respectively. The produced energy for the first case for both LV grids is around one third compared to the curtailment case.

In general, the total losses in the LV grids are higher when the solar production is higher. This will also be the situation for all the cases here, but an interesting observation is that even though the production is around 3 times higher in the case with curtailment, the loss is just a bit higher compared to the first case. This is because the production is curtailed when it is at its highest, and this will also be the time when the loss is the highest. However, it must be stressed that we only account for electrical losses in the grid, and not the loss due to curtailment.

Table 2: Total capacity on PV cells, total produced solar energy and total loss in the LV grid for the case where PV cells are added until the voltage violate the planning limits, PV cells is added with curtailment to avoid violating the voltage limit and when an OLTC is used for the same reason. The results are given for two LV grids connected to two different load points in the MV grid.

Bus for LV grid	Case	Total capacity	Total produced energy	Total loss
49	Until full	$175\ kW_p$	$196\ MWh$	$20\ MWh$
	Curtailment	$640\ kW_p$	$590\ MWh$	$24\ MWh$
	OLTC	$640\ kW_p$	$720\ MWh$	$28\ MWh$
101	Until full	$65\ kW_p$	$73\ MWh$	$15\ MWh$
	Curtailment	$290\ kW_p$	$280\ MWh$	$19\ MWh$
	OLTC	$290\ kW_p$	$320\ MWh$	$23\ MWh$

4   PV in the MV grid

Next, the goal is to see what the consequences in the MV grid will be if there is a large-scale deployment of solar panels in all the underlying LV grids. Further on it is assumed that all the distribution transformers (between the MV and LV grid) have OLTCs and that the thermal capacity of the transformers is sufficient, such that all houses can have PV on rooftops without causing problems in the LV grid. The same assumptions as above is applied to find the numbers of household and to add PV cells. Only on bus 49 and 101 an explicit LV grid is added. For the rest of the buses in the MV grid, PVs are added based on the load on the bus, and with the assumption that the voltage limit will not be violated in the LV grid. The impact on the MV grid will be equivalent to an explicit representation of the LV grid. To add a detailed grid on all the load buses would not provide more information as many assumptions would have been required to match the load levels of the MV grid. The two LV grids added will demonstrate possible interactions. For the other load points, that do not have an explicit LV grid modelled, the losses in these grid needs to be modelled. How this is done is explained in Appendix A.3.

4.1 Results

When including PV in every household in the LV grids, the voltage is not violating the planning limit in the MV grid at maximum production, and the line capacities are also not exceeded. In Figure 5 the voltage magnitude for one summer day at 12am is shown for both the case where PV is only added to one LV grid (left: PV cells in LV grid at bus 49, right: PV cells in LV grid at bus 101), the blue line, and when there is PV in every LV grid, the orange line. These curves show the voltage only at the upstream (LV and MV) buses from a given load point in the LV grid, rather than all the buses in the grid, thus the electrical distance from the main feeder increases from left to right. In the two LV grids that are modelled, the voltage is a bit higher than if there is PV production in only one LV grid, but still within the limit. This shows that PV cells can be installed on the roofs of every household within this MV grid without exceeding the voltage limit, provided that active measures, such as the implementation of OLTCs, are taken in the LV grid.
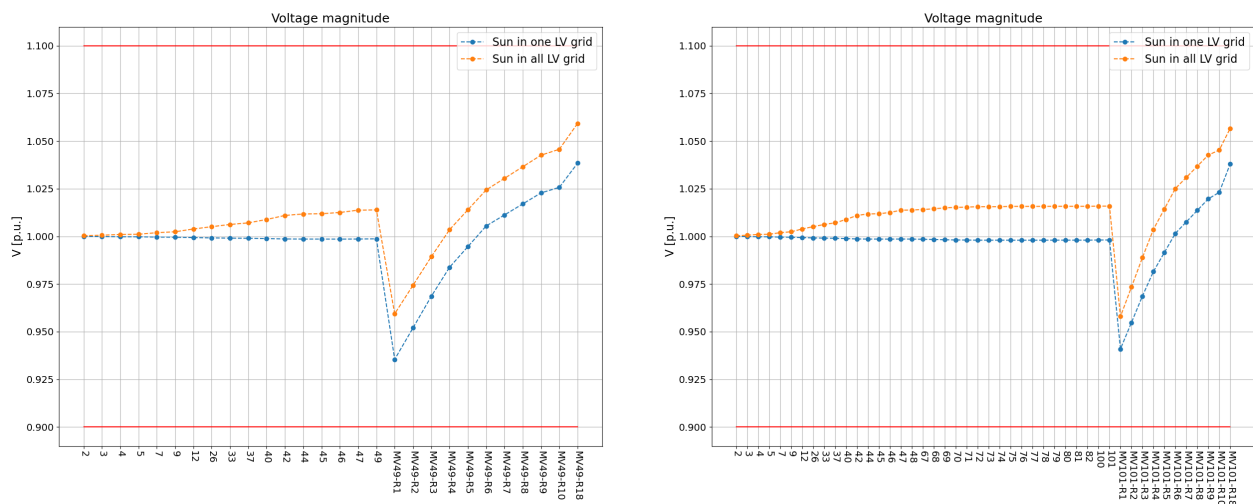
Figure 5: Voltage magnitude of the upstream buses from a given bus in a LV grid (LV grid at bus 49 is shown on the left and LV grid at bus 101 is shown on the right) for when PV cells is installed in only the shown LV grid (blue) and when PV cells are installed on every household in MV grid.

The total capacity of the solar panels is $15{,}8\ MW_p$. The PV production led to a maximum export of $11{,}3\ MW$ to the upstream grid. For comparison, the maximum import to the distribution grid is only $5{,}24\ MW$. The total produced solar energy is $17{,}7\ MWh$.

5   Charging stations, PV and BESS in the MV grid

This chapter considers new connections in the MV grid. The new loads and productions are
- Two FCSs
- One HPCS
- A PV plant
- A battery energy storage system (BESS)

We assume that the HPCS, PV plant and BESS are owned by the same customer and are connected to the same bus.

5.1   Charging stations in the MV grid

First, new consumption is added. To know where in the grid capacity is available to add new consumption, a capacity map is used. The capacity map considers both voltage limits and thermal capacity of transformers and lines in the grid. How the capacity map is generated is described in detail in reference [17]. This capacity map considers AMS data and not just maximum load and coincidence factors. It is possible to generate a capacity map for every operating state in the grid, but in this case, we want to find the limiting capacity and thus we consider the hours with the highest load, and then the limiting capacity on every bus is given in the capacity map. The capacity map for the reference grid is shown in Figure 6.
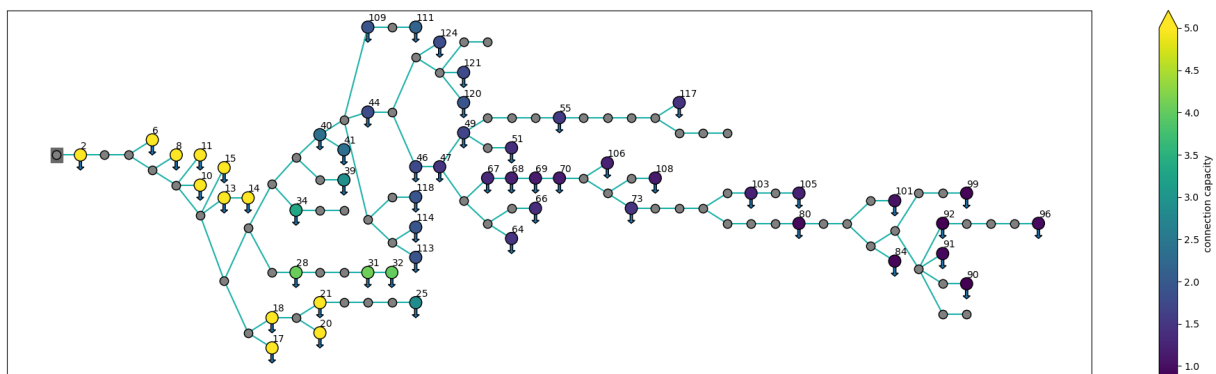

Figure 6: Capacity map for the MV reference grid

A capacity map can be used to see where there is available capacity in the grid in case of a need for a new connection. Assuming that the maximum load of the new connection is known, the map can be used to show where it can be connected. As an example, a FCS for private cars wants to connect to the grid. The maximum load of the charging station is $2.3\ MW$. The capacity map can now be used to see where there is available capacity for more than $2.3\ MW$. This is shown in Figure 7. The green buses represent the buses where there is available capacity and the red buses where there is not available capacity.
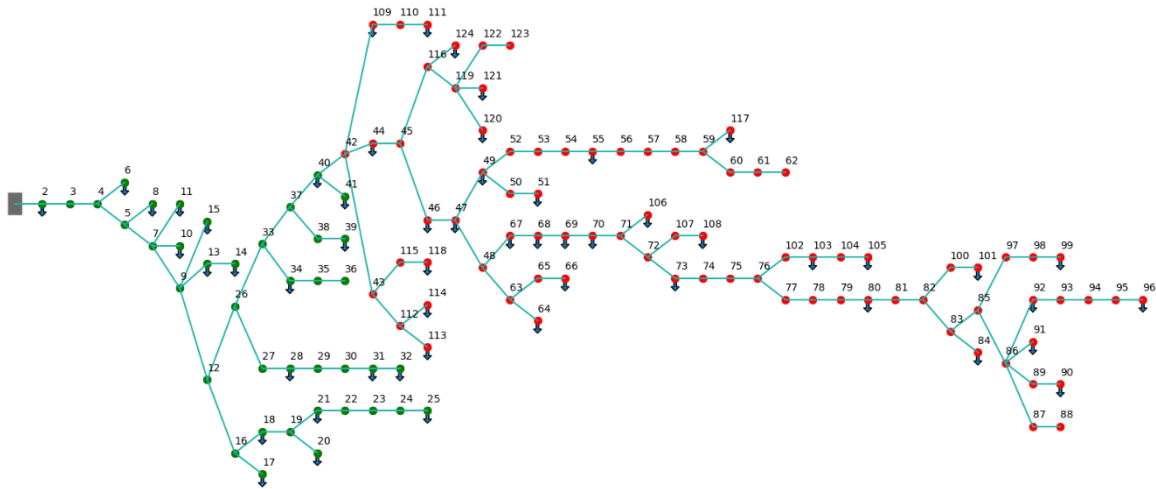
Figure 7: Capacity map of the CINELDI MV reference grid showing (green buses) where a new connection with peak load 2.3 MW can connected without violating voltage limits or thermal limits. The red buses shows where these limits could be violated.

From Figure 7 it is seen that there is enough available capacity at bus 2 to bus 41 for this connection request. The FCS connects to bus 30. Further, another FCS wants to connect to the grid. This charging station has a peak load of $2.9\ MW$. Since there already is a new customer connected to the grid, a new capacity map must be generated. This leads to a similar result, but this time the buses with available capacity are 2 to 22. This FCS therefore connects to bus 22. The next customer that wants to connect to the grid is a charging station for heavy-duty transportation, a high-power charging station (HPCS). This has a peak load of $2.5\ MW$. Now, when generating the capacity map, the grid has capacity for this charging station only at bus 2 to bus 6 and bus 8. In this case, it is assumed that the HPCS still wants to connect to bus 29, which will lead to problems in the grid.

5.1.1 Results

When the HPCS connects to the grid (bus 29) there will be only 5 hours where the voltage is lower than the planning limit and/or the thermal capacity of the line is exceeded.
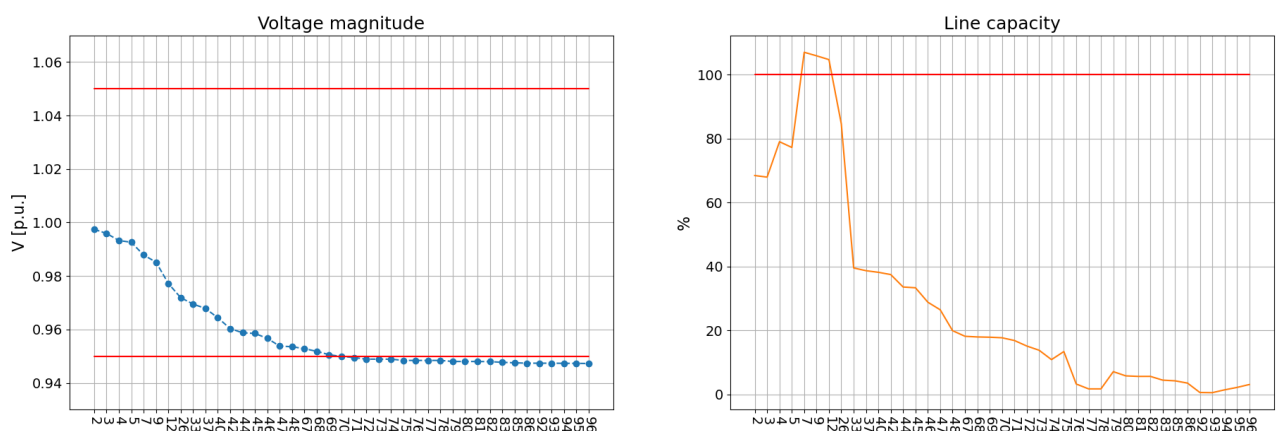

Figure 8: Voltage magnitude (left) and thermal capacity of the lines (right) for the upstream buses from bus 96 for one of the hours where these properties exceed their respective limits.

The voltage and the thermal capacity for one of these hours are shown in Figure 8. In this figure, only the buses upstream from bus 96 are considered. From this figure, it is seen that the voltage on the buses further out in the grid gets too low, and that the lines closest to the slack bus are overloaded. One way of solving this problem is by adding a battery at the charging station. In this memo, it will not be discussed what the best solution is to solve this problem, it is just assumed that a battery is installed. To model the use of the battery, optimization methods are used. This is explained in Appendix A.4. The result for the battery is shown in Figure 9. Here, it is possible to see that the battery is used to cover parts of the load in the hours where the load is the highest. Since the load only is too high a few hours, the usage of the battery will also only be a few hours, and value-stacking by using the battery for other services will probably be needed to make the investment profitable.
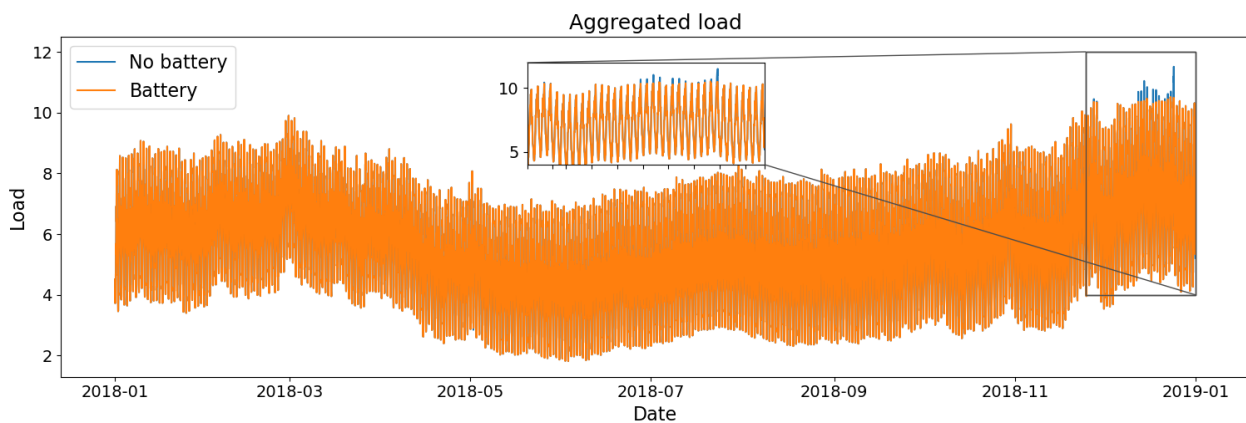

Figure 9: Aggregated load for reference grid, two FCS and one HPCS with (orange) and without (blue) a battery.

5.2   PV plant in the MV grid

The HPCS operator plans to install a PV plant and a BESS on the same substation as the HPCS. We assume that the PV plant will have an installed capacity of $5\ MW_p$. In addition to calculating hosting capacity for demand, the capacity map [17] can be used to find hosting capacity for PV production. The operating states limiting the PV hosting capacity are hours around noon during summer, when the irradiation is high while the load demand is relatively low. The PV capacity map is shown in Figure 10 and the capacity at bus 29, which is the location of the HPCS, is larger than 10 MW. Thus, the PV plant can be connected without further measures.

We assume that the production profiles from rooftop PV in the LV grids, and the PV plant in the MV grid are perfectly correlated. The correlation of the PV production profiles will be slightly lower than 100% due the effects of terrain, clouds and different orientation of PV cells. Assuming perfect correlation is a conservative choice since the production peaks will be simultaneous, and thus the impact on the grid is overestimated. Even with perfect correlation of production, the integration of PV cells on all residential rooftops, as described in Chapter 4, combined with the PV plant do not cause voltage problems or congestions in the test system.
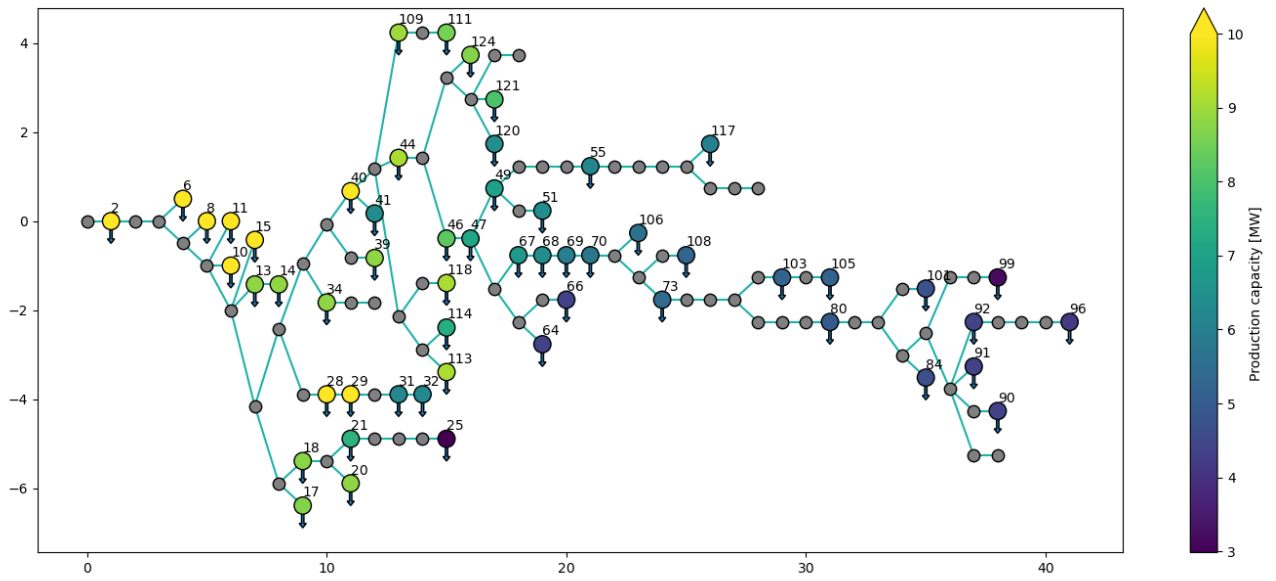
Figure 10: PV hosting capacity map for the CINELDI reference grid.

6   Electrical losses

This chapter summarizes the effect on electrical losses from the new elements introduced in the system. Figure 11 shows both the total annual losses and how these are divided between the LV and MV grid levels. From left to right in the figure, new elements are added in the same order as presented in chapters 4-5: 1) Large scale deployment of rooftop PV. 2) FCSs and HPCSs. 3) And finally, the PV plant. The results shown in Figure 11 are also presented in Table 3. Note that the BESS is not included in the analysis since the simple peak-shaving strategy which was implemented only activates the BESS a few hours during the year, thus having negligible impact on the total loss.
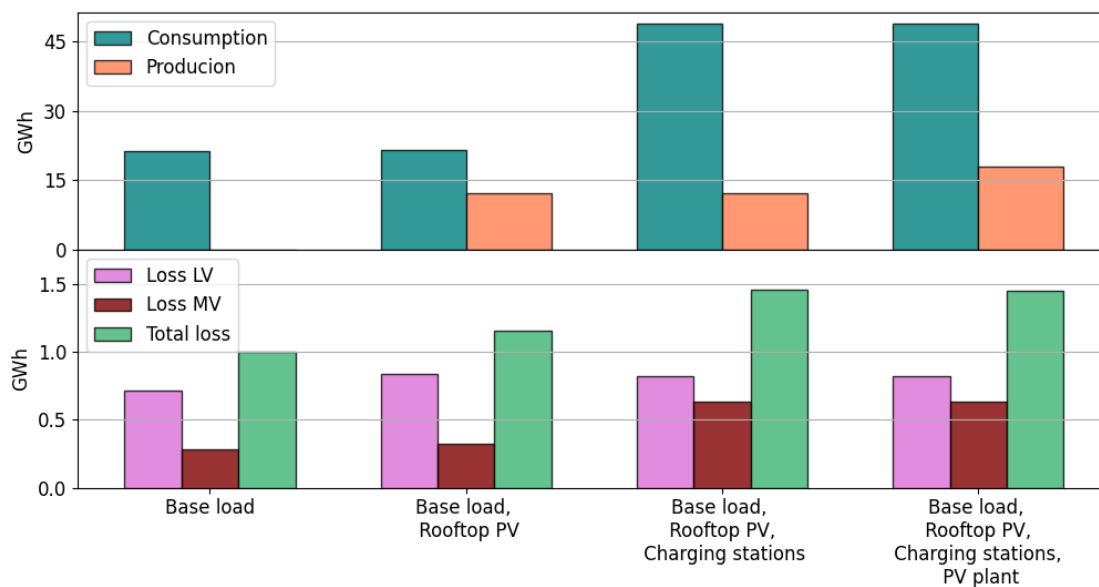

Figure 11: Annual consumption and production (top). And annual loss in the LV and MV grid (bottom) for different combinations of new elements in the system.

Table 3: Annual consumption and production. And annual loss in the LV and MV grid for different combinations of new elements in the system.

Load/production elements	Loss LV [GWh]	Loss MV [GWh]	Total loss [GWh]	Consumption [GWh]	Production [GWh]
Base load	0.715	0.282	0.997	21.3	0.0
Base load, rooftop PV	0.836	0.323	1.16	21.3	12.2
Base load, rooftop PV, charging stations	0.820	0.637	1.46	48.8	12.1
Base load, rooftop PV, charging stations, PV plant	0.819	0.632	1.45	48.8	18.0

We find that the rooftop PV increases the total annual losses in both the MV and LV grid, and the total losses in the system increase by 16% compared to the base-case. The increased losses can be explained by a low degree of self-consumption: Although the PV production is located close to consumers, the residential loads have a seasonal trend which is negatively correlated with the PV production. When the

electric heating demand is high during winter, the PV production is low, and during summer there is a considerable surplus of power exported to upstream grid levels. This reversed power flow is the cause of the increased losses.

Not surprisingly, the load from the HPCS and FCSs increase the total losses. Since the charging stations are connected directly to the MV grid, the losses only increase on the MV level. The charging stations are connected at strong nodes which are electrically close to the main feeder, and thus the added losses are modest relative to the added load: the annual consumption in the system increases by 229% whereas the annual losses only increase by 26%.

Installing the PV plant leads to a slight decrease in losses on both grid levels. This happens because a considerable part of the production is consumed locally by the HPCS. In summary, we observe that EV charging stations can achieve a higher degree of self-consumption of PV generation than residential customers. Therefore, co-localizing PV installations and charging stations can have a positive impact on the electrical losses in the distribution grid.

There is an established method [18] for estimating the socio-economic cost of electrical losses which is used by Norwegian DSOs in grid investment planning. Simply put, the cost of losses is calculated from two parameters: the annual energy loss, and the annual peak power loss. The energy loss leads to lost revenue for actors on the power market which must be covered by the grid owners, and the peak power loss incurs investments in grid capacity locally and upstream in the grid. The current method for cost calculation is however not valid when local generation leads to export of power from the distribution grid to higher voltage levels. The results presented in this memo underscores the need for research on the socio-economic impact of electrical losses accounting for distributed generation.

7   Conclusions

This case study has made use of tools and knowledge from CINELDI and affiliated research projects. The case has illustrated a future distribution grid with a substantial growth in local PV production and load demand due to EV charging. The research demonstrated that the expected future demand and production causes congestions and voltage violations in the grid. The main result from the work is that these problems can be mitigated by active measures without grid reinforcement. The results are specific to the test system that was used. However, the observed impact of new load and production on the grid and the effect of active measures are widely applicable. The results from the different parts of the case study are summarised and discussed in the following.

The case study included PV on all residential buildings in addition to a larger PV plant. The results show that the extensive amount of PV production leads to violations of upper voltage limits in the low voltage grid, which cannot be solved by traditional manual tap changing. Two active measures were tested individually which successfully solved the voltage violations: Automatic PV curtailment and OLTCs. Curtailment reduced the annual PV production with 15% compared to using OLTCs. We have not assessed the economic cost of the two alternatives. However, it is reasonable to assume that curtailment is considerably less expensive than installing OLTCs on all substations. The possible benefit of using OLTCs is that all the energy from the PV is transferred to the grid. A third alternative, which has not been investigated, is for customers to install private BESS to store energy for later use when the local demand is higher.

The case study included multiple EV charging stations: two fast charging stations for private cars (FCS) and a high-power charging station (HPCS) for heavy-duty vehicles. Without active measures, the added load results in overload on lines and violation of lower voltage limits in the MV grid. PV production compensates for both these problems when the solar radiation is high. However, a large portion of the time, PV production in Norway is virtually zero and thus the problems remain. The problems were successfully solved by adding a larger battery energy storage system together with the HPCS. The BESS was modelled using a very simple peak-shaving strategy which resulted in the battery being used only a few hours for one year. We have not investigated other potential benefits of a BESS, batteries can for instance participate on intraday and reserve markets and provide voltage support to the grid by reactive power supply [19]. Moreover, the BESS is only one possible solution to make the connection of the HPCS viable. Other relevant alternatives include non-firm/conditional connection agreements or reducing the overall capacity of the charging station. It is up to the charging station operator to choose the best alternative.

From the analysis of electrical losses, we make some general observations: Extensive deployment of PV panels on residential rooftops is likely to increase losses in the distribution grid due to the negative temporal correlation of electrical heating demand and PV production in Norway. Furthermore, FCSs and HPCs connected at strong nodes in the MV grid has a relatively low impact on losses in the distribution grid, and co-localization of PV generation and charging stations increases self-consumption while decreasing electrical losses. We show that the full-scale deployment of PV panels on residential rooftop, and the PV plant causes considerable export of power from the distribution grid at times with high irradiance. Therefore, we stress the need for research on how the socio-economic impact of electrical losses changes in the future energy system.

A limitation with this study is that the local distribution grid is studied in isolation without considering the effect on the upstream grid. Although the problems in the local distribution grid due to added load in terms of EV charging and local production from PV were solved using active measures, the altered power flow may cause congestions in the regional distribution grid. Especially if similar load

development occurs in multiple distribution grids simultaneously. In addition to possible congestions, higher shares of converter-based generation such as PV and wind power is a challenge to voltage and frequency stability in the transmission system. The use of active measures allows grid operation with less margin to physical limits which affects the reliability of supply. We encourage future research to address how the reliability of supply, i.e. the probability and consequence of power interruptions, is affected by new operating conditions.

References

[1]   I. B. Sperstad, O. B. Fosso, S. H. Jakobsen, A. O. Eggen, J. H. Evenstuen, og G. Kjølle, «Reference data set for a Norwegian medium voltage power distribution system», *Data in Brief*, s. 109025, mar. 2023, doi: 10.1016/j.dib.2023.109025.

[2]   «Benchmark Systems for Network Integration of Renewable and Distributed Energy Resources», *Electra*, 2014.

[3]   «Nasjonal transportplan 2018–2029 (Melding til Stortinget)», Samferdselsdepartementet. [Online]. Tilgjengelig på: https://www.regjeringen.no/contentassets/7c52fd2938ca42209e4286fe86bb28bd/no/pdfs/stm20 1620170033000dddpdfs.pdf

[4]   «Budsjettforlik mellom Ap/Sp og SV 2024».

[5]   «NVEs svar på oppdrag om solkraft og annen lokal energiproduksjon», NVE, feb. 2024. [Online]. Tilgjengelig på: https://www.nve.no/media/16752/notatet-nves-svar-paa-oppdrag-om-solkraft-og-annen-lokal-energiproduksjon.pdf

[6]   «DSOs Fit for 55: Challenges, practices and lessons learnt on connecting renewables to the grid», DSO Entity.

[7]   *Directive (EU) 2023/1791 of the European Parliament and of the Council of 13 September 2023 on energy efficiency and amending Regulation (EU) 2023/955 (recast) (Text with EEA relevance)*, bd. 231. 2023. Åpnet: 8. februar 2024. [Online]. Tilgjengelig på: http://data.europa.eu/eli/dir/2023/1791/oj/eng

[8]   L. Thurner *mfl.*, «Pandapower—An Open-Source Python Tool for Convenient Modeling, Analysis, and Optimization of Electric Power Systems», *IEEE Transactions on Power Systems*, bd. 33, nr. 6, s. 6510–6521, nov. 2018, doi: 10.1109/TPWRS.2018.2829021.

[9]   I. B. Sperstad, O. B. Fosso, S. H. Jakobsen, A. O. Eggen, J. H. Evenstuen, og G. Kjølle, «Reference data set for a Norwegian medium voltage power distribution system», 18. oktober 2022, *TechRxiv*. doi: 10.36227/techrxiv.21258513.v1.

[10]   «Technical Brochure 575: Benchmark Systems for Network Integration of Renewable and Distributed Energy Resources», CIGRE, 2014.

[11]   L. M. Engan, «Undersøkelse av tilknytningskapasitet i distribusjonsnettet ved utbygging av solkraft», 2023.

[12]   «Forbruk, produksjon og installert effekt», Elhub. Åpnet: 4. mars 2024. [Online]. Tilgjengelig på: https://elhub.no/data/forbruk-og-produksjon/

[13]   «Renewables.ninja». Åpnet: 9. juli 2024. [Online]. Tilgjengelig på: https://www.renewables.ninja/

[14]   S. Pfenninger og I. Staffell, «Long-term patterns of European PV output using 30 years of validated hourly reanalysis and satellite data», *Energy*, bd. 114, s. 1251–1265, nov. 2016, doi: 10.1016/j.energy.2016.08.060.

[15]   H. M. Dalen, B. Halvorsen, og B. M. Larsen, «Strømproduksjon fra solcelleanlegg i norske husholdninger. Analyser av plusskunder basert på Elhub», Statistisk sentralbyrå.

[16]   K. K. Fjær, V. Lakshmanan, B. N. Torsæter, og M. Korpås, «Heavy-duty electric vehicle charging profile generation method for grid impact analysis», i *2021 International Conference on Smart Energy Systems and Technologies (SEST)*, sep. 2021, s. 1–6. doi: 10.1109/SEST50973.2021.9543135.

[17]   I. Bjerkebæk, «Evaluation of Available Connection Capacity in Medium Voltage Distribution Grids», SINTEF Energy Research, Project Memo CINELDI WP6, 2024.

[18]   SINTEF Energy Research, «Tapskostnader», i *Planleggingsbok for kraftnett*, REN / SINTEF Energy Research, 2019.

[19]   R. Rana, I. B. Sperstad, B. N. Torsæter, og H. Taxt, «Economic assessment of integrating fast-charging stations and energy communities in grid planning», *Sustainable Energy, Grids and Networks*, s. 101083, jun. 2023, doi: 10.1016/j.segan.2023.101083.

[20] A. Tutvedt, «Webinar: Automatisk spenningsregulering med AMS», The Norwegian Smart Grid Centre, 31. august 2023. [Online]. Tilgjengelig på: https://smartgrids.no/arrangementer/webinar-automatisk-spenningsregulering-med-ams/

[21] «Nøkkeltall for nettselskapene - NVE». Åpnet: 12. juli 2024. [Online]. Tilgjengelig på: https://www.nve.no/reguleringsmyndigheten/publikasjoner-og-data/data-og-noekkeltall/noekkeltall-for-nettselskapene/

[22] W. E. Hart, J.-P. Watson, og D. L. Woodruff, «Pyomo: modeling and solving mathematical programs in Python», *Math. Prog. Comp.*, bd. 3, nr. 3, s. 219–260, sep. 2011, doi: 10.1007/s12532-011-0026-8.

[23] *Gnu Linear Programming Kit (GLPK)*. (2012). [Online]. Tilgjengelig på: https://www.gnu.org/software/glpk/

Appendix A Description of simulation methods

A.1 Simulation of PV curtailment

The modelling of curtailment is done by finding the maximum upstream net power flow in the LV grid that gives a voltage under the given limits. To find a general load limit, the two LV grids are looked at separately (without the MV grid) and for two different tap-changing levels (see 2.1). Since we are only analysing solar production within a single LV grid in this case, this represents a worst-case scenario. In practice, higher levels of solar production are often possible without exceeding voltage limits, as consumption in the rest of the MV grid reduces the overall voltage in the LV grid.
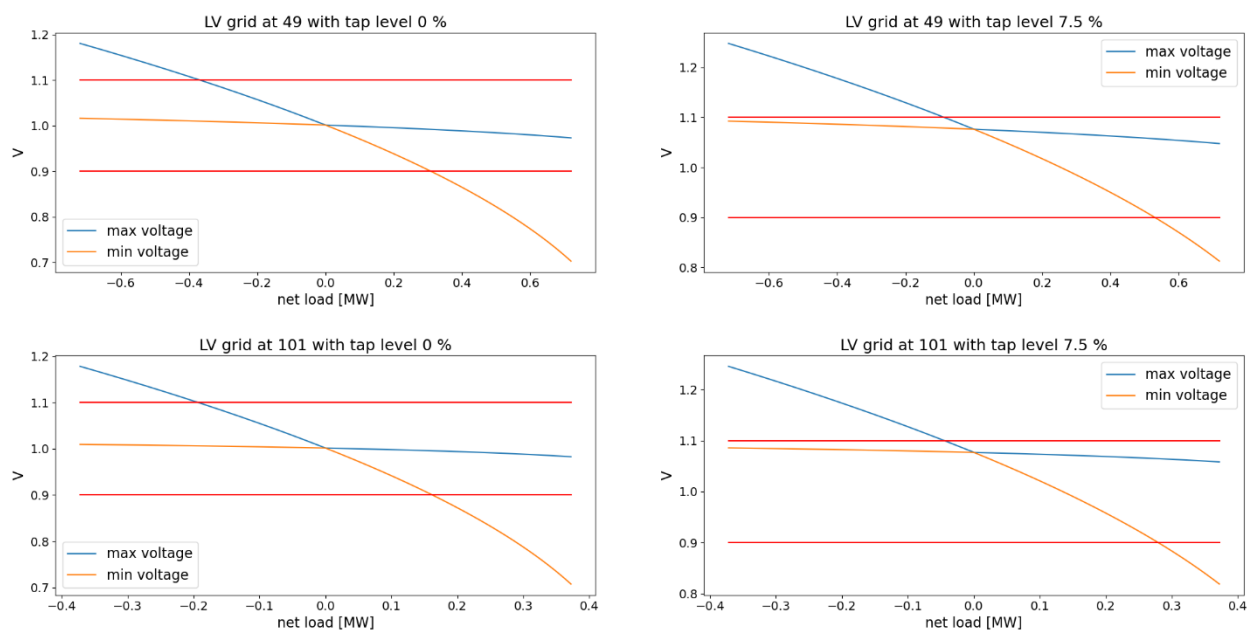

Figure 12: Shows how the voltage depends on the net load in the LV grid at bus 49 (upper plots) and 101 (lower plots) for tap level 0 % (left) and 7,5 % (right). The blue curve is the maximum voltage in the grid, the orange the minimum voltage, and the red lines are the voltage limits.

Curtailment is in this case done equally reducing the PV production for each customer. Since all the load points in this case have the same timeseries for both consumption and production, just multiplied with a different scaling factor, the curtailment is easily found by just scaling down the timeseries. Since the two LV grids are different the net load will also be different. Figure 12 shows the correlation between the net load and the minimum and maximum voltage in the two LV grids for the two different tap-changing levels.
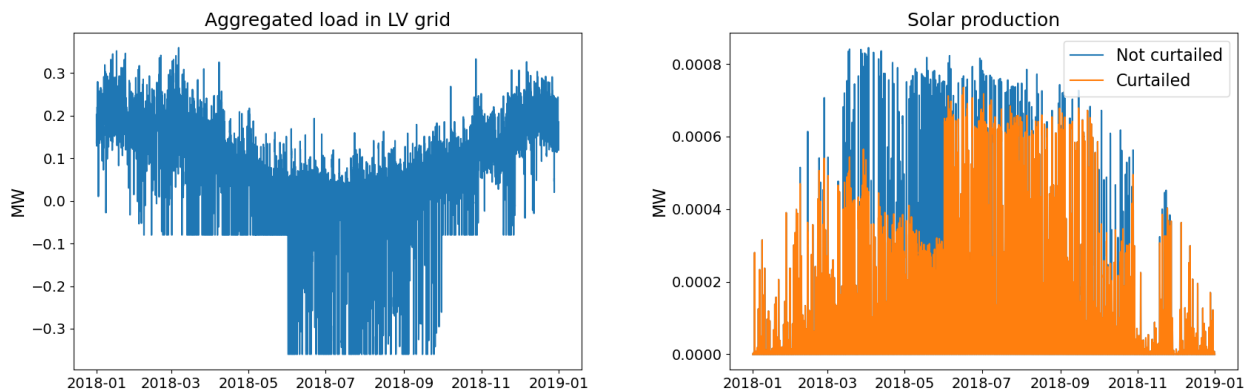
Figure 13: Shows the aggrerated load with curtailed solar production (left) and the curtailed (orange) and not curtailed (blue) solar production with the same capacity on the PV cells.

In Figure 13 the result of the curtailment is shown. The left figure shows the aggregated load in one of the LV grids when curtailed solar production is included, and the right figure shows the solar production with and without curtailment. In the figures one can also clearly see the difference for the different tap-changing levels during summer and winter.

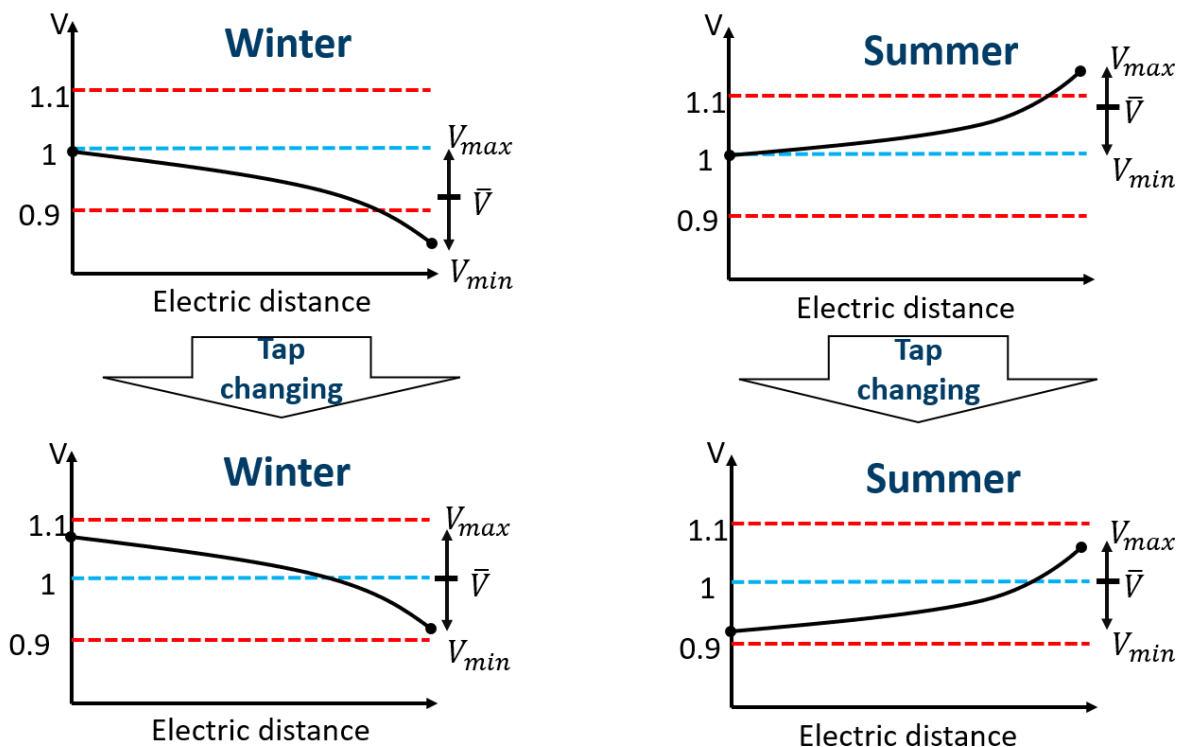## A.2 Simulation of on-load tap changers

Figure 14: Illustration of voltage problems in the LV grid in summer and winter with tap-changing to restore the voltage within limits.

Without tap-changing, voltage problems occurred in both LV-grids in the test system (buses 49 and 101). During winter when the load demand is high, the voltage drops below 0.9 p.u. towards the end of the radial. When PV production is added to all rooftops as described in chapter 3, the voltage exceeds 1.1 p.u. during periods with high PV production and low demand in the summer. The different voltage problems during summer and winter are illustrated in the topmost subfigures in Figure 14. To simulate an OLTC, a heuristic approach was implemented which proved to solve the voltage violation throughout the year. This approach tries to restore the mean voltage in the grid to 1 p.u. The mean voltage $\overline{V}$ is in this case defined as the mean of the maximum V_{max} and minimum voltage V_{min} in the grid

$$\overline{V} = \frac{V_{max} + V_{min}}{2}.$$

The rationale behind this choice is illustrated in the two bottom subfigures in Figure 14: keeping $\overline{V}$ at 1 p.u. gives the smallest deviations of V_{min} and V_{max} from the nominal voltage. For the OLTCs, a tap step of 1% was assumed, and the maximum and minimum tap settings were $\pm 10\%$.

The voltage levels in the grid can in practice be read using AMS [20]. In this case study however, voltage levels must be found from power flow calculations. To restore $\overline{V}$ to 1 by tap-changing, $\overline{V}$ must first be found for the tap setting from the previous time step, and then the best tap setting for the current time step must be found. This approach requires at least two power flow calculations for each time step. To avoid running an excessive number of power flow calculations, an approximate tap-setting was determined based on the net load in the LV grid, i.e. the sum of demand and production. To find a relation between net load and the approximate tap settings, the LV grid was studied alone without being connected to the MV grid. The load in the grid was uniformly scaled on all buses for a range of load values, and the best tap setting for each load value was found. Note that this approximation does not account for different distributions of load on the buses in the LV grid, or voltage deviations at the connecting bus in the MV grid. The voltage levels for different load scaling factors with and without tap-changing are shown in Figure 15. Except for a few hours of the year, the approximate tap setting was sufficient to eliminate voltage problems. For the few hours where the voltage problems remained, the tap setting was determined by finding $\overline{V}$ from power flow calculations, and the voltage problems could then be solved.
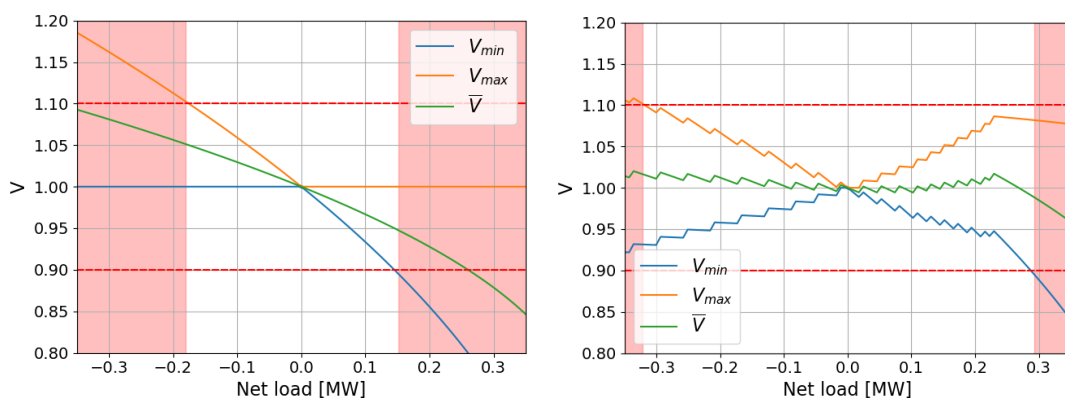

Figure 15: Voltage levels with (right) and without (left) tap changing. The red shaded areas mark the load values where voltage violations occur.

A.3 Approximation of electrical losses in LV-grids

For the two LV grids connected at buses 101 and 49 in the MV grid, electrical losses can be found directly from power flow calculations. However, there are also LV grids under the remaining load points in the LV grid which are not included in the test system. We do however approximate the loss in these grids, and the approximation is described in this subsection.

Let P denote the load flow from the MV grid to the LV grid and let P_Σ denote the sum of load and production at all buses in the LV grid. The electrical loss in the LV grid is then $|P - P_\Sigma|$. We define the relative power loss, η as

$$\frac{P}{P_\Sigma} = 1 + \eta$$

For the LV grid at bus 49 in the MV grid, we scale the load over a range of values, solve the power flow equations and determine η. We use curve-fitting to find a 2nd order polynomial giving η as a function of $x = P_\Sigma/P_{\Sigma,max}$, where $P_{\Sigma,max}$ is the annual peak load for the LV grid. The parameters of the polynomial are

$$h(x) = a_1\, x + a_2\, x^2,$$
$$a_1 = 0.059 \text{ and } a_2 = 0.013.$$

Using this empirical relation, we approximate the loss in the LV grids which are not part of the network model as

$$\eta(x) = h(x) \cdot P_{\Sigma,max}.$$

Now, $P_{\Sigma,max}$ refers to the maximum annual load at each load point in the MV grid. Studying $h(x)$, we see that:
- The loss is 7.2% at peak load: $h(x = 1) = 0.072$,
- The loss is zero when the net load is zero $h(x = 0) = 0$,
- And the loss is 4.6% when the net load is $-P_{\Sigma,max}$, i.e. if the PV production is so high that there is a reverse power flow with equal magnitude as the annual peak load.

It must be stressed that this is only a reasonable approximation when the net load is in the range of $P_\Sigma \in [-P_{\Sigma,max},\ P_{\Sigma,max}]$, and when the relative distribution of the load on the different buses does not vary too much throughout the year.

The average and maximum loss for the CINELDI reference grid using the approximation for losses in the LV grids are reported in Table 4. And the duration curves for losses in the LV and MV grid is shown in Figure 16. The average loss in distribution grids in Norway is 3.8% in 2023 [21] which is similar to the value of 3.62% which we found for our test system.

Table 4: Average and maximum loss for the MV reference system before adding new load and production. The values are relative to the total load in the system.

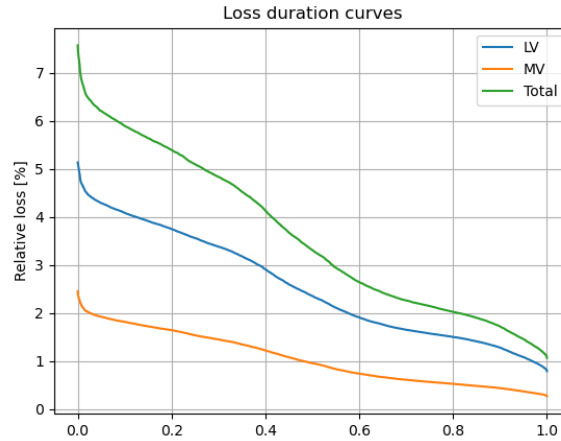| Voltage level	Average loss [%]	Maximum loss [%]
LV	2.59	5.26
MV	1.07	2.52
Combined	3.62	7.58

Figure 16: Loss duration curves for the MV and LV grids.

A.4 Load shifting using BESS

The load shifting using the BESS was modelled using Pyomo which is an open source software package for optimization with Python [22]. The objective of the BESS is to minimize the peak load in the grid

$$\min P_{max},$$

where

$$P_{max} \geq P_{\Sigma,t} \quad \forall t,$$

and $P_{\Sigma,t}$ is the sum of load and production for hour t in the entire test system including both the MV and LV buses. The following constraints were defined:

$$P_\Sigma + P_{gen} - P_{demand} - P_{bat} = 0,$$

This is the energy balance where P_{gen} denotes PV production, P_{demand} denotes load demand and P_{bat} denotes battery charging power.

$$SOC_t \geq 0,$$

$$SOC_t \leq E_{max},$$

These constrains imply that the state of charge (SOC) of the battery is nonnegative and not exceeding the maximum energy capacity E_{max}.

$$SOC_0 = SOC_T,$$

This is a periodic boundary condition for the state of charge (SOC), where T denotes the last time step.

$$-C_{dis} \leq P_{bat},$$

$$C_{ch} \geq P_{bat},$$

These constraints specify the charging C_{ch} and discharging capacity C_{dis} of the battery.

$$SOC_t - SOC_{t-1} = \begin{cases} \dfrac{P_{bat}}{\eta_{ch}}, & P_{bat} \geq 0 \\ P_{bat} \cdot \eta_{ch}, & P_{bat} < 0 \end{cases}$$

This constraint is the energy balance of the battery, where η_{ch} is the charging/discharging efficiency factor which was set to 95%. The open source GLPK solver [23] was used with Pyomo to solve the optimization program.